Supporting Information

Low-energy Interlayer Phonon Assisted Carriers Recombination in Z-Scheme van der Waals Heterostructures for Photocatalysis

Hejin Yan,[a] Qiye Guan,[a] Hongfei Chen,[a] Xiangyue Cui,[a] Zheng Shu,[a] Dan Liang,[a] Bowen Wang,[a] Yongqing Cai[a]*

[a]Joint Key Laboratory of the Ministry of Education, Institute of Applied Physics and Materials Engineering, University of Macau, Taipa, Macau, China

Corresponding Author

Yongqing Cai* E-mail: yongqingcai@um.edu.mo

Computational details

The DFT simulations were performed based on the Vienna *ab initio* simulation package (VASP) package.[1, 2] The generalized gradient approximation (GGA) of Perdew-Burke-Ernzerhof form (PBE) was adopted to treat the electronic exchange-correlation energy. Both the projector augmented (PAW) functions and HSE06 functions were used to calculate the band structure and optical properties. All atomic structures were fully relaxed until energies and forces were

coverage to 10^{-6} eV and 1×10^{-4} eV/Å respectively with a cutoff energy of 500 eV in the plane-wave expansion. The vdW interaction was also considered by the empirical DFT-D3 method. The unit cells of the TMD and WSi_2N_4 were optimized at first by using a 15 × 15 × 1 Monkhorst-Pack k-mesh. Then, the Brillouin zone integration was sampled using the 3 × 3 × 1 k-points mesh for structure optimization and a denser 5 × 5 × 1 k-points mesh for electronic properties calculation for the heterostructures. A vacuum layer of 15 Å was added in the z direction to avoid the impact of pseudo images. The harmonic interaction force constants (2nd) and phonon dispersion spectrum were determined using the density-functional perturbation theory (DFPT) scheme by the Phonopy package.[3]

Calculation details for NAMD. After the structure optimization at 0 K, the 4×4×1 supercells were adopted for the WSi_2N_4 monolayer and WSi_2N_4/TMD heterostructures to suppress artificially introduced "phonon bottleneck". Due to the big system and high computational load, only the phonon modes at the Γ point were considered for both heterostructures. All systems were equilibrated through repeated velocity rescaling for 5 ps at 300 K, and another 5 ps adiabatic molecular dynamic trajectories were generated within the subsequent microcanonical ab initio molecular dynamics using a time step of 1 fs. The molecular dynamics were performed at Γ point. The nonadiabatic molecular dynamics (NAMD) calculations were performed by using the semi-classical decoherence induced surface hopping (DISH) approach implemented in PYXAID code.[4] The decoherence effects were considered through the semi-classical DISH scheme which describes the interactions between the quantum nuclei and electronic subsystem. In order to mimic the charge dynamic on a long-time scale, the obtained nonadiabatic Hamiltonians were involved in an iteration process. The first 1000 geometries were selected as the initial conditions, and 2000 sampling numbers for each initial structure to realize the statistical average. Baring mind a similar band structure and orbital composition obtained by the PBE and HSE06 levels, a scissor operator is applicable within the NAMD simulation to compensate the band gap lowering. The scissor operators of 0.45 eV and 0.3 eV were applied for the MoS_2/WSi_2N_4 and $MoSe_2/WSi2N_4$ heterostructures, respectively to match the HSE06 derived band gap.

Calculation details for HER and OER. Considering the longer carrier lifetime and more suitable band alignment of the WSi_2N_4/MoS_2 heterostructure, the same 4×4×1 WSi_2N_4/MoS_2 supercell

was used for exploring the thermodynamics of the HER and OER processes, which take place at the WSi_2N_4 and MoS_2 side, respectively. Additional vacancy models were constructed through substituting one N or S atom by one vacancy on the surface. The Gibbs free energy, ΔG, under standard condition is defined as[5]:

$$\Delta G = \Delta E + \Delta E_{ZPE} - T\Delta S - ne - U_{RHE} \quad (1)$$

where ΔE is the total energy change obtained from DFT calculation; ΔE_{ZPE} is the change in zero-point energy derived from the vibrational frequency; ΔS is the difference in entropy; n is the number of proton/e^- pairs consumed within a certain step; and U_{RHE} is the contribution from external potential. The OER process involves four elementary oxidation steps and expressed as[6]:

$$* + H_2O \longrightarrow *OH + H^+ + e^- \quad (2)$$

$$*OH \longrightarrow *O + H^+ + e^- \quad (3)$$

$$*O + H_2O \longrightarrow *OOH + H^+ + e^- \quad (4)$$

$$*OOH \longrightarrow * + O_2 + H^+ + e^- \quad (5)$$

where the $*$ represents the active site on the pristine catalysts surface, and the $*OH$, $*O$, and $*OOH$ denote the radial adsorbed on the surface. Meanwhile, the HER process can be decomposed into two one-electron steps, as follow[6]:

$$* + H^+ + e^- \longrightarrow *H \quad (6)$$

$$*H + H^+ + e^- \longrightarrow * + H_2 \quad (7)$$

HER and OER catalytic activity of WSi_2N_4/MoS_2. The catalytic activities for the HER and OER of the WSi_2N_4/MoS_2 heterostructure are investigated by the Gibbs free energy. The nitrogen vacancy (V_N) and selfie vacancy (V_S) contained surfaces are also considered for the HER and OER processes, respectively, as the single atom vacancy is a common method to enhance the catalytic ability. In Figure S8a, ΔG_{H*} for the pristine WSi_2N_4/MoS_2 of 0.17 eV is even smaller than that of 0.36 eV in V_N contained surface. Under a bias external potential of 0.4 V, the HER

catalytic occurs on the WSi_2N_4/MoS_2 surface spontaneously. For the OER process, the free energy evolution in the WSi_2N_4/MoS_2 is an uphill process at 0 V. Meanwhile, these elementary steps become spontaneously in the V_S contained surface at an equilibrium potential of 1.23 V. In summary, the constructed Z-scheme WSi_2N_4/MoS_2 heterostructure is an applicable photocatalyst for water splitting.

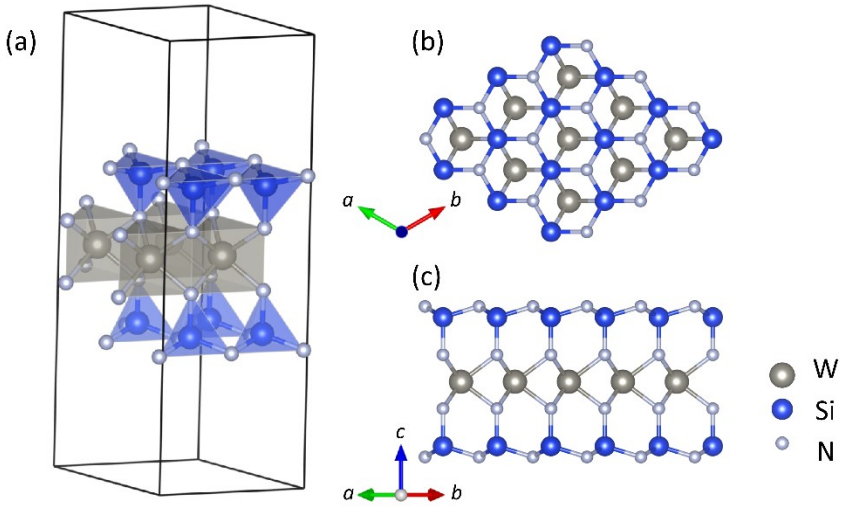

Figure S1. (a) Honeycomb like crystal structures of the WSi_2N_4 from (b) top and (c) side view.

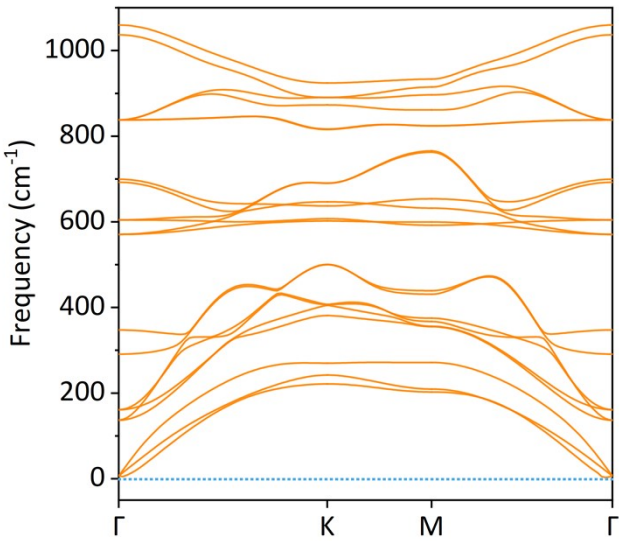

Figure S2. Phonon dispersion of WSi_2N_4 based on a 4×4×1 supercell.

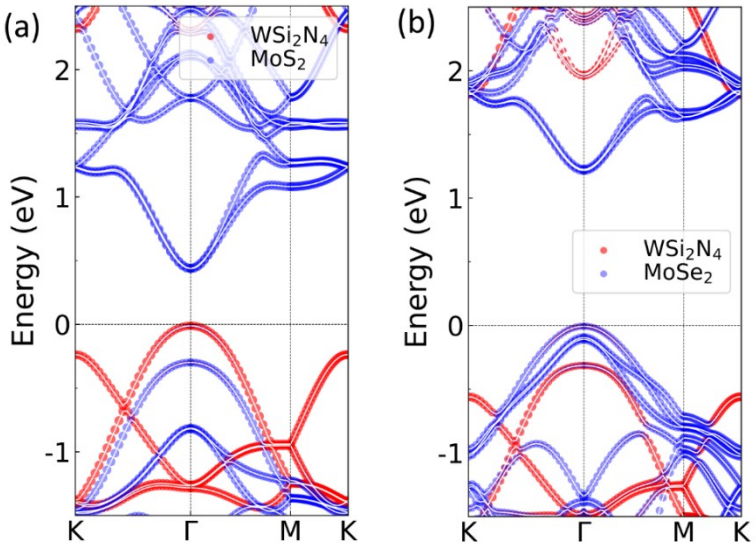

Figure S3. Element projected band structures of the WSi_2N_4/MoS_2 and $WSi_2N_4/MoSe_2$ heterostructures from the PBE calculations

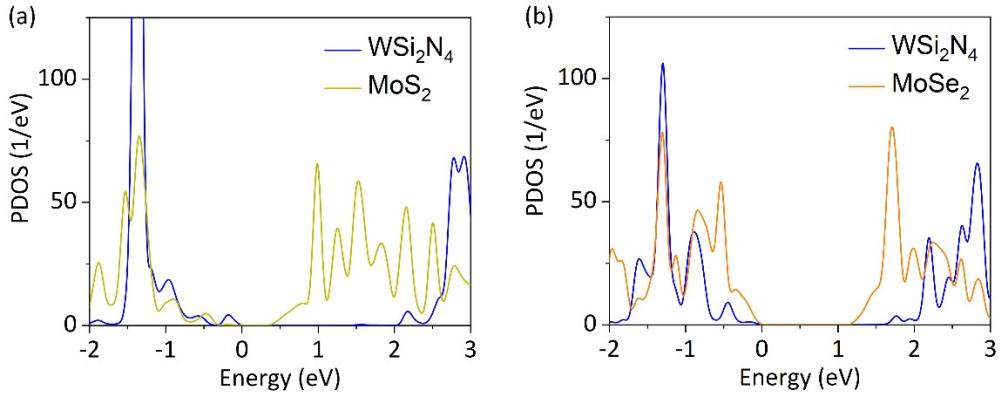

Figure S4. Partial density of states (PDOS) of the (a) WSi_2N_4/MoS_2 and (b) $WSi_2N_4/MoSe_2$ heterostructures from the PBE calculations.

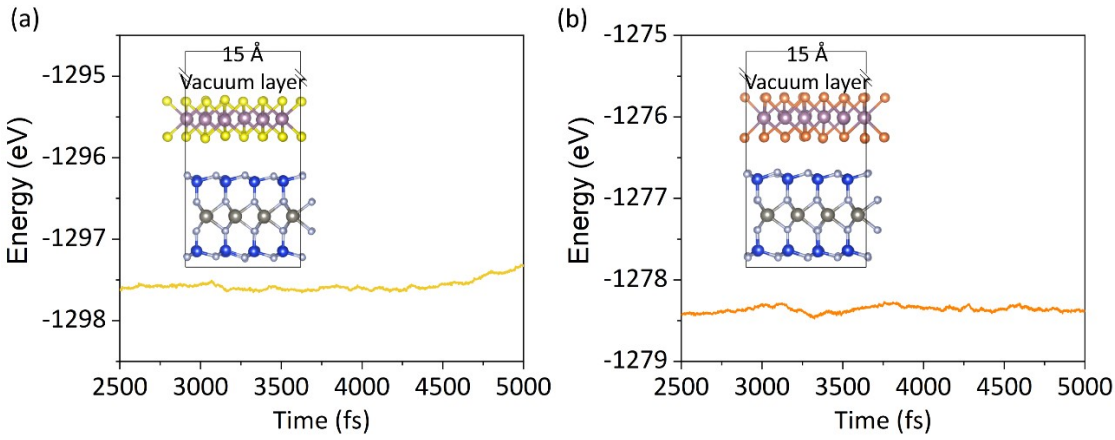

Figure S5. Evolution of the total energy of the heterostructures WSi_2N_4/MoS_2 (a) and WSi2N4/MoSe2 (b) within the last 2.5 ps during the NVE AIMD equilibrium process. The inserted pictures are the snapshots of the heterostructures at 5.0 ps.

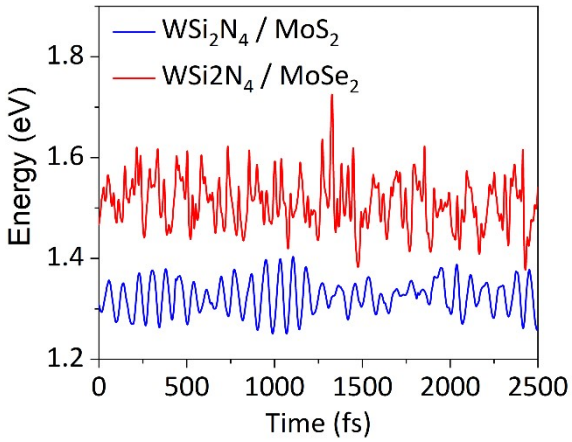

Figure S6. Evolution of the band gap of the heterostructures WSi_2N_4/MoS_2 and WSi2N4/MoSe2 within the NAMD simulation. The band gap is rescaled by the scissor operators with the HSE06 results as the reference.

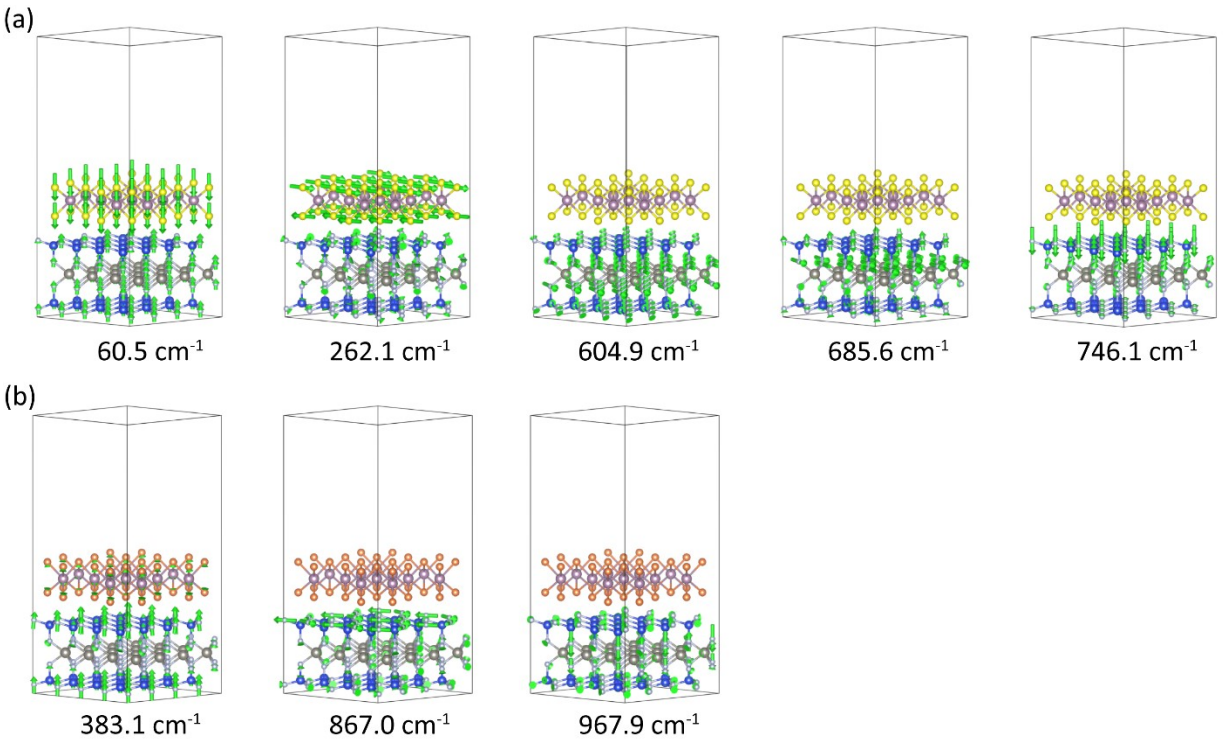

Figure S7. Related phonon modes for charge recombination in the (a) WSi_2N_4/MoS_2 and (b) $WSi_2N_4/MoSe_2$ heterostructures.

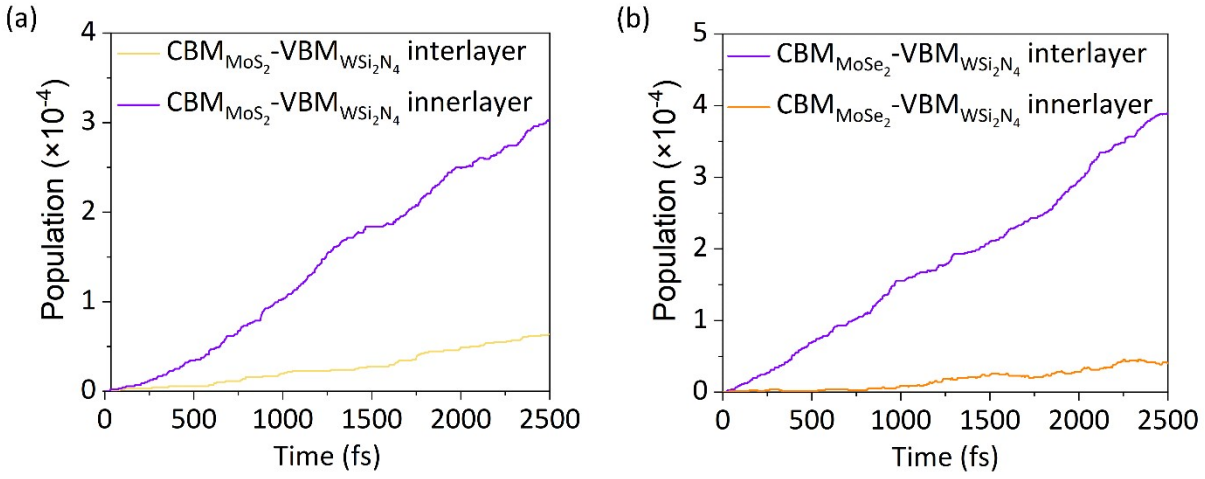

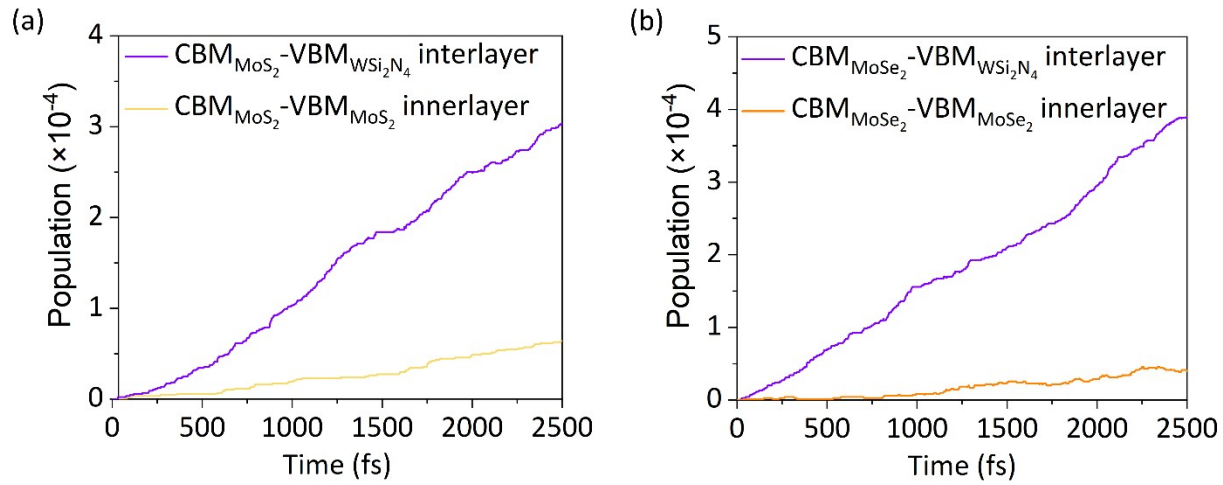

Figure S8. Electron-hole recombination through interlayer ($^{CBM_{TMD}-VBM_{WSi_2N_4}}$) and innerlayer ($^{CBM_{TMD}-VBM_{TMD}}$) channels in the (a) WSi_2N_4/MoS_2 and (b) $WSi_2N_4/MoSe_2$ heterostructures.

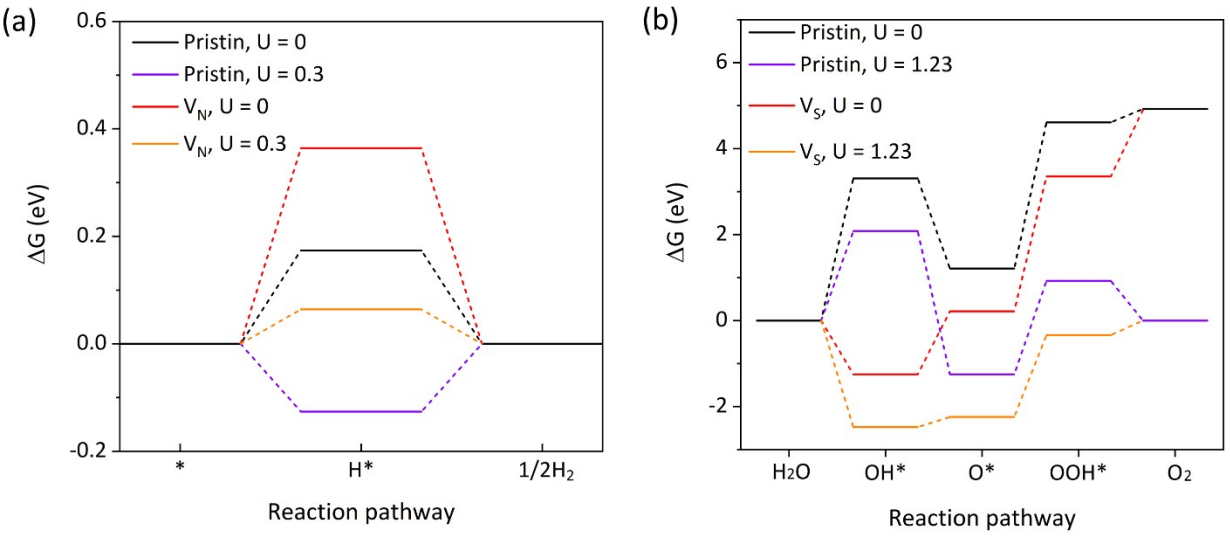

Figure S9. The Gibbs free energy profiles of the (a) HER and (b) OER on the WSi_2N_4/MoS_2 heterostructure.

Table S1. Hot electron relaxation time of each orbital.

Orbital	τ (fs)
CBM+3	587
CBM+4	542
CBM+5	544
CBM+6	437
CBM+7	433
CBM+8	411
CBM+9	401
CBM+10	393

References

1. G. Kresse and J. Furthmüller, *Comput. Mater. Sci.*, 1996, **6**, 15-50.
2. G. Kresse and J. Hafner, *Phys. Rev. B*, 1993, **47**, 558.
3. A. Togo and I. Tanaka, *Scripta Mater.*, 2015, **108**, 1-5.
4. A. V. Akimov and O. V. Prezhdo, *J. Chem. Theory Comput.*, 2013, **9**, 4959-4972.
5. R. Bar-Ziv, P. Ranjan, A. Lavie, A. Jain, S. Garai, A. Bar Hen, R. Popovitz-Biro, R. Tenne, R. Arenal and A. Ramasubramaniam, *ACS Applied Energy Materials*, 2019, **2**, 6043-6050.
6. J. Meng, J. Wang, J. Wang, Q. Li and J. Yang, *J. Mater. Chem. A*, 2022, **10**, 3443-3453.